Snapshots of the maltose transporter during ATP hydrolysis

Michael L. Oldham and Jue Chen[1]

Department of Biological Sciences, Purdue University, Howard Hughes Medical Institute, 240 Martin Jischke Boulevard, West Lafayette, IN 47907

Edited by Douglas C. Rees, California Institute of Technology/Howard Hughes Medical Institute, Pasadena, CA, and approved July 11, 2011 (received for review June 1, 2011)

ATP-binding cassette transporters are powered by ATP, but the mechanism by which these transporters hydrolyze ATP is unclear. In this study, four crystal structures of the full-length wild-type maltose transporter, stabilized by adenosine 5′-(β,γ-imido)triphosphate or ADP in conjunction with phosphate analogs BeF_3^-, VO_4^{3-}, or AlF_4^-, were determined to 2.2- to 2.4-Å resolution. These structures led to the assignment of two enzymatic states during ATP hydrolysis and demonstrate specific functional roles of highly conserved residues in the nucleotide-binding domain, suggesting that ATP-binding cassette transporters catalyze ATP hydrolysis via a general base mechanism.

membrane protein | transition state | ground state

ATP-binding cassette (ABC) transporters are large membrane protein complexes powered by ATP (1). In prokaryotes, ABC transporters are survival factors mediating the uptake of nutrients and the efflux of antimicrobial agents and virulence factors. In humans, 48 ABC transporters are identified that transport a variety of compounds and are responsible for diseases including cystic fibrosis, cholestasis, and multidrug resistance in cancer (2). ABC transporters, both importers and exporters, contain two transmembrane domains (TMDs) that form a substrate translocation pathway and two nucleotide-binding domains (NBDs) that bind and hydrolyze ATP. Structures of intact transporters show that an inward-facing state, where the substrate translocation pathway is accessible from the cytoplasm, coincides with an open NBD dimer in which the ATPase active sites are separated (3–8). Closure of the NBD dimer in the presence of ATP is concomitant with reorientation of the substrate translocation pathway from an inward-facing to an outward-facing configuration (7, 9, 10). Several sequences are highly conserved among NBDs for ATP hydrolysis, including: (*I*) the Walker A motif with a consensus sequence of GxxGxGKST, where x represents any amino acid; (*ii*) the Walker B motif, which has four hydrophobic residues followed by a negatively charged residue; (*iii*) the D loop, containing a conserved aspartic acid; (*iv*) the LSGGQ loop, or the signature motif, diagnostic of ABC ATPases; (*v*) the Q loop, named after its invariable glutamine; and (*vi*) the switch region that contains a highly conserved histidine residue. However, uncertainty exists regarding the functional role of these motifs and the chemistry of ATP hydrolysis. For example, based on studies of isolated NBDs, the acidic residue immediately following the Walker B motif, a glutamate in most ABC transporters, was suggested by several groups to act as a general base to polarize the hydrolytic water molecule (11, 12). But in a different model, this glutamate residue functions, instead, to orient the switch histidine while the ATP is hydrolyzed via substrate-assisted catalysis rather than by a general base mechanism (13). High-resolution structures of catalytic intermediates of a complete ABC transporter would be valuable to establish the chemical mechanism of ATP hydrolysis. Unfortunately, all known structures of either isolated NBD dimers or intact transporters in complex with ATP have been obtained with either active site mutations and/or in the absence of the Mg^{2+} ion (10, 13–16). Although alteration of key catalytic residues or omission of the metal cofactor was necessary to prevent ATP hydrolysis during crystallization, these changes might, in turn, alter the position of the triphosphate moiety and neighboring residues, thus yielding an inaccurate depiction of the active site conformation.

The maltose transporter from *Escherichia coli* has been studied for several decades as the prototype to elucidate the fundamental mechanism of ABC transporters. Four proteins are required to transport maltose and other maltodextrins across the cytoplasmic membrane in *E. coli*, including a periplasmic maltose-binding protein (MBP); two integral membrane proteins, MalF and MalG; and two copies of the cytoplasmic ATPase component, MalK (17). To obtain crystal structures of the wild-type (WT) maltose transporter that better approximate conformational states along the trajectory of ATP hydrolysis, the nonhydrolyzable ATP analog, adenosine 5′-(β,γ-imido)triphosphate (AMP-PNP), as well as a number of metal complexes were used in this study to stabilize catalytic intermediates. These structures provide insights into the mechanism by which ABC transporters hydrolyze ATP.

Results and Discussion

Stabilizing Complexes of the MBP-MalFGK$_2$ with γ-Phosphate Analogs. Complexes of MBP-MalFGK$_2$ were formed prior to crystallization by incubating WT MalFGK$_2$ with MBP, maltose, AMP-PNP or ATP plus a γ-phosphate mimic [vanadate (VO_3^{3-}), beryllium fluoride (BeF_3^-) or aluminum fluoride (AlF_4^-)]. Following ATP hydrolysis, the γ-phosphate mimic substitutes for the leaving inorganic phosphate before ADP has been released (18). Crystals diffracted anisotropically to approximately 2.2- to 2.4-Å resolution along the best direction (Tables S1 and S2). The final electron density maps, after anisotropic correction of the X-ray data (19), were of excellent quality and allowed accurate positioning of the nucleotide, Mg^{2+} ion, and water molecules at the active site (Fig. S1).

The overall structures of MBP-MalFGK$_2$ cocrystallized with AMP-PNP, ADP-BeF_3, ADP-VO_4, or ADP-AlF_4 are essentially identical to each other and to that of the outward-facing conformation obtained using ATP and a catalytically inactive mutant MalFGK$_2$(E159Q) (Fig. S2*A*) (10). The root-mean-square deviation (rmsd) of the entire complex (1,870 Cα positions) ranges between 0.2–0.9 Å between any two structures. In this conformation, MBP binds to MalF and MalG in an open conformation and the two MalK subunits form a closed dimer, with two nucleotides bound along their common interface (Fig. 1*A*). Residues at the

Author contributions: M.L.O. and J.C. designed research; M.L.O. performed research; M.L.O. and J.C. analyzed data; and M.L.O. and J.C. wrote the paper.

The authors declare no conflict of interest.

This article is a PNAS Direct Submission.

Freely available online through the PNAS open access option.

Data deposition: Coordinates and structure factors have been deposited in the Protein Data Bank, www.pdb.org (PDB ID codes 3RLF, 3PUX, 3PUV, and 3PUW).

See Commentary on page 15015.

[1]To whom correspondence should be addressed. E-mail: chenjue@purdue.edu.

This article contains supporting information online at www.pnas.org/lookup/suppl/doi:10.1073/pnas.1108858108/-/DCSupplemental.

ATP-binding sites superimpose well with the 2.8-Å E159Q mutant structure, indicating that the E159Q mutation and omission of Mg^{2+} ion in crystallization did not cause any distortion at the active site (Fig. S2*B*). The structures of the analog-trapped WT protein are of higher resolution; accordingly, detergent and lipid molecules and additional waters could be modeled along with the transporter complex. Several water molecules were found inside the transmembrane cavity, making hydrogen bonding contacts with maltose (Fig. 1*B*).

Molecular Details at the Active Site. It is well known that ATP hydrolysis proceeds by direct in-line attack of the ATP γ-phosphate group by a hydrolytic water molecule, through formation of a pentacovalent transition-state intermediate (Fig. 2*A*) (20, 21). In the transition state, the geometry of the γ-phosphate changes from tetrahedral to trigonal bipyramidal, with three oxygen atoms at the equatorial plane, and the β/γ phosphate bridging oxygen and the water nucleophile at the axial positions (Fig. 2*A*) (20, 21). What do we observe in our high-resolution structures of the maltose transporter? Electron density maps with the nucleotide and analogs omitted for the AMP-PNP or ADP-BeF_3 structures reveal a tetrahedral geometry about the γ-phosphate and the γ-phosphate analog (Fig. 2*B*). Therefore, these two structures represent the ground state, enzyme-substrate complex (the Michaelis complex) of an ABC transporter. In contrast, the trigonal bipyramidal or octahedral geometry observed in the omit maps for the ADP-VO_4 or ADP-AlF_4 structures, respectively (Fig. 2*C*), recapitulate the γ-phosphate undergoing nucleophilic attack by a water molecule. Therefore, the transition state can be modeled by the complex structures stabilized by ADP-VO_4 and ADP-AlF_4.The stereochemistry of the analogs observed here are consistent with high-resolution structures of GTPases (22, 23) and F_1-ATPases (24–27).

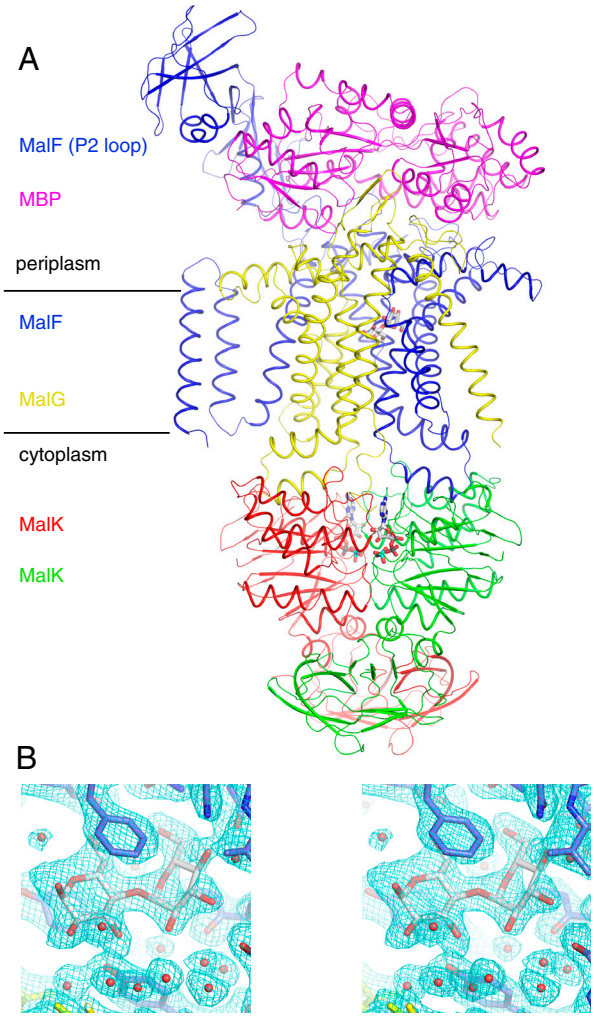

Fig. 1. Structure of the maltose transporter in an outward-facing conformation. (*A*) Ribbon representation of the overall ADP-VO_4 structure. Maltose and ADP-VO_4 are shown in stick model. (*B*) Stereo view of maltose bound to MalF (blue) and surrounding water molecules within the transmembrane cavity of the AMP-PNP structure, together with a nonweighted $2F_o - F_c$ electron density map countered at 1.2σ.

Detailed comparison of these structures shows that at the ATP-binding site all residues are essentially superimposable (Fig. 3*A*). In both states, the active site is stabilized by a network of interactions from ATP and Mg^{2+} to residues highly conserved among ABC transporters (Fig. 3 *B–D*). The ATP β-phosphate forms hydrogen bonds with five consecutive residues in the Walker A motif (Fig. 3*B–D*). The γ-phosphate interacts with the Walker A, the Q-loop, and the switch histidine of one NBD and the LSGGQ motif of the other NBD, thus, tightly tethering the two NBDs. The Mg^{2+} ion is coordinated by the Walker A S43, the Q-loop Q82, two water molecules, and the β- and γ-phosphates, linking these important structural elements together (Fig. 3*B–D* and Fig. S3). In previous structures of isolated NBDs, the function of a conserved glutamine residue (Q82 in the maltose transporter) in the Q loop has been inconsistent, probably due to the absence of the TM subunits, which interact extensively with the Q loop. Here, we observe in the structures of an intact transporter that the Q-loop glutamine interacts with the metal ion and the γ-phosphate of ATP, and thus plays an essential role in ATP hydrolysis (Fig. 3).

Consistent with the chemistry of ATP hydrolysis, the structural differences between the ground state and the transition state lie in the conformation of the γ-phosphate and the presence of an attacking water molecule (Fig. 3 and Fig. S3). In the AMP-PNP and ADP-BeF_3 structures, the distance between the γ-phosphate and the bridging oxygen of the β-phosphate is around 1.7 Å, approximating that of a covalent linkage in the ground-state ATP (Fig. 3*B* and Fig. S3*A*). Electron density corresponding to the hydrolytic water is absent in both the AMP-PNP and ADP-BeF_3 structures (Fig. S1), suggesting that the ground-state conformation has low affinity for the attacking water. In contrast, in the structures trapped with transition-state analogs, a water molecule is observed at both ATPase sites of the ADP-AlF_4 structure, positioned 2.3 Å from the γ-phosphate and in-line with the β/γ bridging oxygen of the inorganic phosphate leaving group (Fig. 3*D* and Fig. S3*B*). In the ADP-VO_4 structure, the attacking water is represented by a covalently linked oxygen atom (Fig. 3*C* and Fig. S3*B*). In the transition state, the glutamate residue following the Walker B motif, E159, makes a strong hydrogen bond with the attacking water, consistent with its function to polarize the water nucleophile (Fig. 3 *C* and *D* and Fig. S3*B*). In full-length transporters, mutating this glutamate to glutamine, a mimic of the protonated form of glutamate, abolishes ATP hydrolysis (28–30), consistent with a strong base at this position being essential for hydrolysis.

Implications to the ATP Hydrolysis Mechanism. Taken together, the active site structure in the ATP ground and transition states support the general base catalysis model, where ATP is hydrolyzed by formation of a pentacovalent intermediate and the hydrolytic water is activated by the acidic residue following the Walker B motif. An alternative mechanism, the substrate-assisted catalysis, was proposed based on studies of the HlyB-NBD where the switch histidine is replaced by alanine (H662A) (13). Comparison of the WT maltose transporter structure with that of HlyB H662A shows that the conserved glutamine residue in the Q loop is displaced in HlyB, likely due to the absence of TMDs (Fig. 4). Furthermore, the sidechain of the catalytic base (E631 in HlyB)

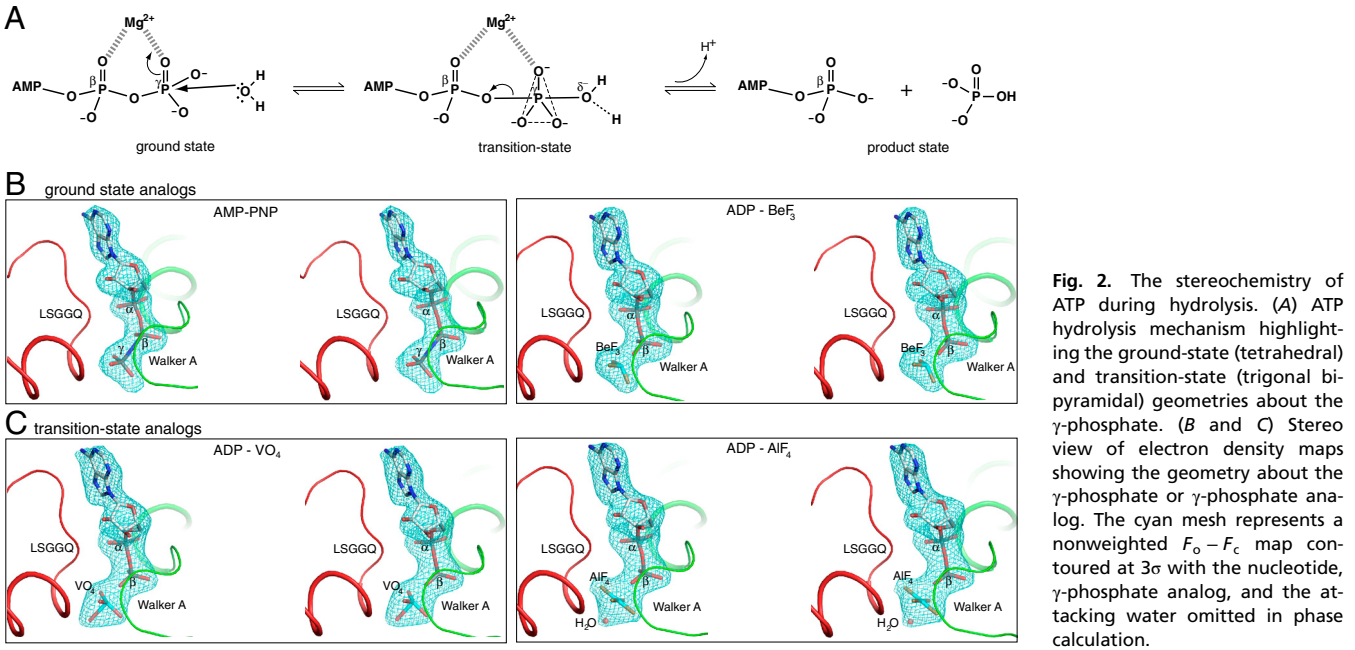

Fig. 2. The stereochemistry of ATP during hydrolysis. (*A*) ATP hydrolysis mechanism highlighting the ground-state (tetrahedral) and transition-state (trigonal bipyramidal) geometries about the γ-phosphate. (*B* and *C*) Stereo view of electron density maps showing the geometry about the γ-phosphate or γ-phosphate analog. The cyan mesh represents a nonweighted $F_o - F_c$ map contoured at 3σ with the nucleotide, γ-phosphate analog, and the attacking water omitted in phase calculation.

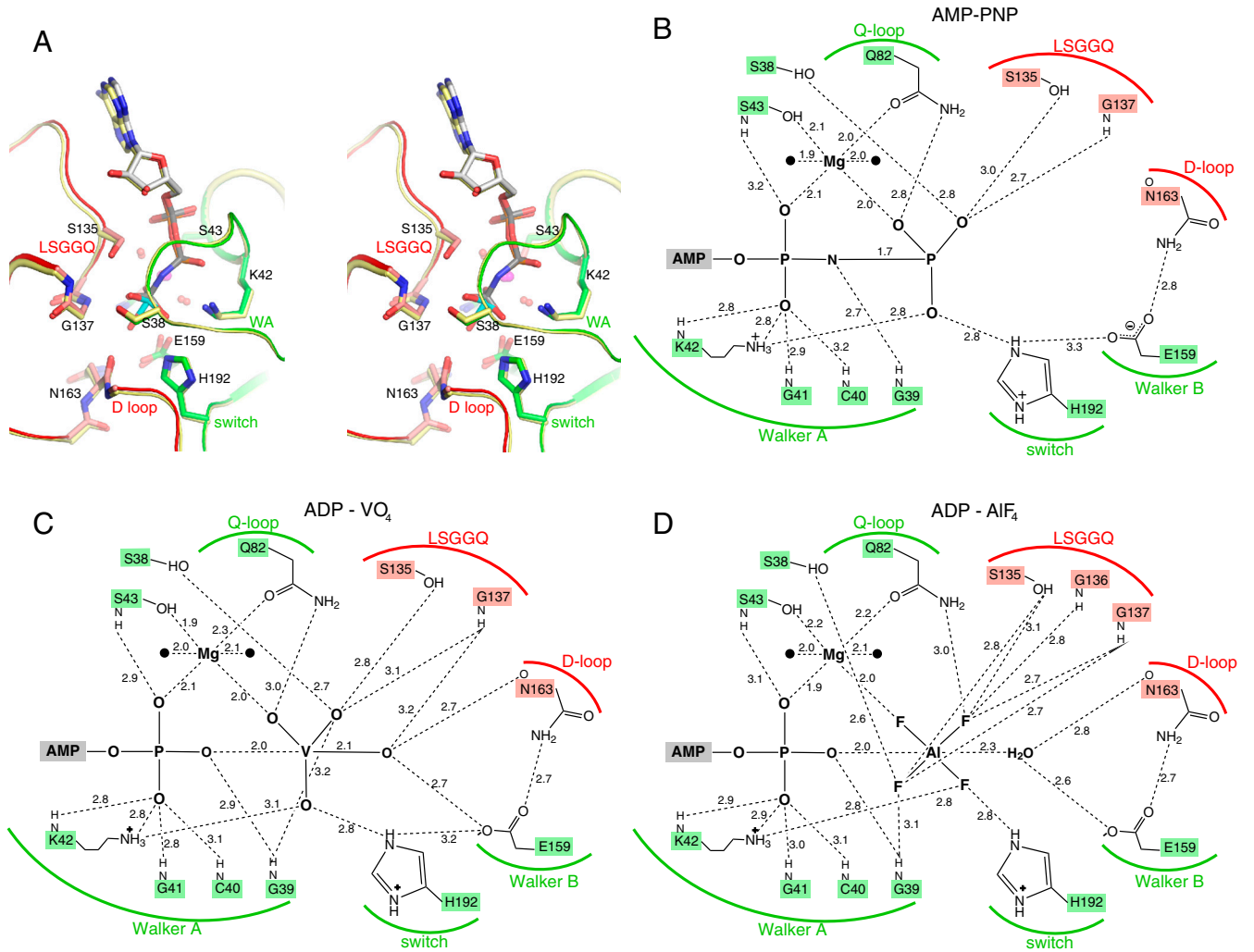

Fig. 3. Molecular details at the catalytic center. (*A*) Stereo view of the AMP-PNP (red and green) and ADP-VO_4 (yellow) trapped structures superpositioned via their Walker A motifs. (*B*, *C*, and *D*) Schematic illustrations showing the coordination of AMP-PNP (ground state), ADP-VO_4, and ADP-AlF_4 (transition state), respectively. Residues from the two MalK monomers are differentiated by color (red and green). Hydrogen bonds (<3.2 Å) and Mg^{2+} ligand interactions are indicated by dashed lines along with their contact distances (in angstroms).

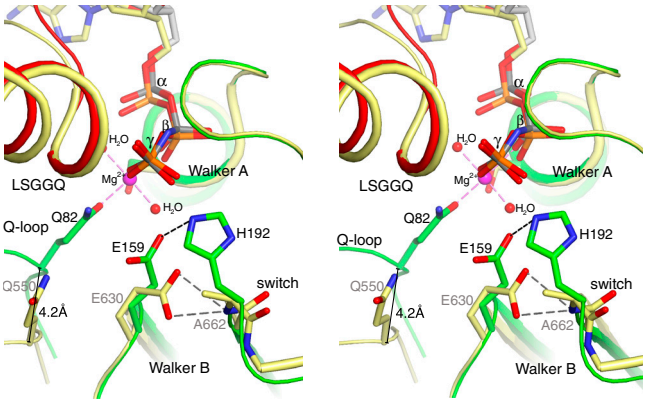

Fig. 4. The catalytic base is displaced in the H662A mutant. Stereo view of the maltose transporter in complex with AMP-PNP (red and green) and HlyB H662A mutant (yellow, Protein Data Bank ID code 1XEF) superpositioned via their Walker A motifs. Contacts made by the catalytic base are indicated by black dashed lines.

is oriented away from the catalytic site, forming, instead, a hydrogen bond with the backbone amide of the substituted A662. In this configuration, E631 is not positioned to deprotonate the attacking water, thus explaining the loss of ATPase activity in this mutant. Although our results argue against the substrate-assisted catalysis model, the structural role of the switch histidine observed in the maltose transporter (Fig. 3 and Fig. 4) supports the conclusion that this histidine functions as a "linchpin" in holding together the γ-phosphate, the attacking water, and the catalytic glutamate for catalysis (13).

An outstanding question for ABC transporters is whether one or two ATPs are hydrolyzed during a single transport cycle. Direct measurements of the stoichiometric ratio of substrate transport to ATP hydrolysis have been complicated by either uncoupled ATP hydrolysis or leakage of substrate from membrane vesicles (reviewed in ref. 31). It was first shown in P-glycoprotein that ADP-VO_4 was trapped in only one of the two nucleotide-binding sites (32), suggesting that hydrolysis occurs only in one site per cycle. Previously, using radioactively labeled ligands, we concluded that maltose was absent in the vanadate-inhibited complex and ADP was trapped at 1:1 molar ratio (33). However, in all of the crystal structures obtained with metal complexes in this study, clear electron density was observed for maltose, two ADP, and two γ-phosphate analog molecules. In addition, in the anomalous difference Fourier density map, calculated with data collected near the anomalous edge of vanadium, clear peaks of similar intensity (10σ) were observed at the position of vanadate in both ATP-binding sites (Fig. S4). The apparent discrepancy between the biochemical and crystallographic data may be due to the differences in experimental conditions. The stoichiometry of maltose and ADP was determined in complexes purified by ion-exchange chromatography in the absence of ligands, whereas the crystals were obtained in the presence of high concentrations of maltose and ADP-VO_4. One possibility is that maltose and/or ADP are partially dissociated from the protein during the purification process, leading to an underestimated stoichiometry determined biochemically. The other possibility is that the occupancy of vanadate in the crystal structure is only 0.5 at each binding site, meaning that only one vanadate is trapped with equal distribution between both sites of the MalK homodimer. Therefore, whether one or two ADP is trapped by vanadate in the maltose transporter remains undetermined.

Conclusions

For ABC transporters, ATP hydrolysis and substrate translocation are coupled through conformational changes that place these two events in synchrony. In the absence of maltose, the transporter rests in a catalytically incompetent conformation due to the separation of the LSGGQ motif from the active site (5). Binding of maltose-loaded MBP and ATP are both required to bring about the conformational changes that result in the opening of MBP for delivery of maltose to the translocation cavity and the closure of the MalK dimer for the hydrolysis of ATP (34, 35).

This work addresses the outstanding question of whether the chemical transition state for ATP hydrolysis produces a different functional state. Here, we show that formation of the transition state does not induce or require any further structural rearrangements; the ground-state and transition-state complexes are in the same outward-facing conformation. Therefore, in ABC transporters, the transition state is only a chemical step for hydrolysis, because it does not have any special functional properties for substrate translocation. ATP hydrolysis is catalyzed through a mechanism in which the acidic residue following the Walker B motif acts as the general base to polarize the attacking water. Because all residues involved in ATP binding and hydrolysis are highly conserved, the chemistry of ATP hydrolysis revealed by the maltose transporter is likely to be a general mechanism of the ABC family.

Methods

Expression and Purification of $MalFGK_2$. $MalFGK_2$ expression and purification were carried out essentially as described earlier (10). Briefly, cells were broken by two passes through a high-pressure homogenizer (Emulsiflex-C5; Avestin). The *E. coli* membrane isolated by centrifugation (80,000 × *g* for 40 min at 4 °C) was resuspended at a total protein concentration of 5 mg/mL in buffer containing 20 mM Tris (pH 8.0), 5 mM MgCl2, 10% glycerol, and 0.3% n-Dodecyl-β-D-Maltopyranoside (DDM, Anatrace). Extracted $MalFGK_2$ was purified on cobalt-affinity resin (Clontech) followed by size-exclusion chromatography (Superdex 200, GE Healthcare) in buffer containing 10 mM Tris (pH 8.0), 200 mM NaCl, and 0.06% n-Undecyl-β-D-maltopyranoside (UDM, Anatrace).

Expression and Purification of MBP. MBP containing a C-terminal 6XHis tag was expressed and purified similarly to a previous study (36). MBP was purified by osmotic shock. In brief, cells were initially resuspended gently in a sucrose buffer. After centrifugation (10,000 × *g* for 10 min at 4 °C), the cell pellet was resuspended in ice-cold 5 mM $MgSO_4$ to disrupt the outer membrane and release MBP to the solution. The resulting spheroplasts were removed by centrifugation, and MBP was further purified by affinity (cobalt-affinity resin; Clontech), ion exchange (Source 15Q; GE Healthcare), and gel-filtration chromatography (Superdex 200; GE Healthcare) at 4 °C.

Cocrystallization with AMP-PNP. $MalFGK_2$ (10 mg/mL in 0.06% UDM) and MBP were mixed at a 1:1.25 molar ratio in the presence of 0.2 mM maltose, 2 mM AMP-PNP, and 2 mM $MgCl_2$. Crystals were grown by mixing the protein sample with the reservoir solution containing 28% polyethylene glycol 400, 200 mM NaCl, 50 mM $MgCl_2$, 100 mM sodium HEPES pH 7.5, at a 1:1 ratio in sitting drops at 20 °C. The crystals grew in 5–6 d and were looped out of the drop and directly frozen in liquid nitrogen.

Cocrystallization with Phosphate Analogs. $MalFGK_2$ (1.5 mg/mL) and MBP were mixed at a 1:1.25 molar ratio in the presence of 0.2 mM maltose and 0.03% UDM. A 2X trapping solution containing 2 mM ATP, 2 mM $MgCl_2$, 0.09% UDM, and either 4 mM aluminum chloride/16 mM sodium fluoride, 4 mM beryllium sulfate/16 mM sodium fluoride, or 1 mM VO_4 was prepared and filtered. Protein samples were mixed with the 2X trapping solution at a 1:1 ratio and were incubated with gentle shaking for 30 min at 22 °C and centrifuged at 100,000 × *g* for 20 min. The protein was concentrated to 12 mg/mL, and crystals were grown by mixing the protein sample with the reservoir solution containing 27% polyethylene glycol 400, 100 mM NaCl, 100 mM $MgCl_2$, 100 mM sodium HEPES pH 7.5, at a 1:1 ratio in sitting drops at 20 °C. The crystals grew in 4–5 d and were looped out of the drop and directly frozen in liquid nitrogen.

Vanadate Preparation. Sodium orthovanadate was dissolved in water, and the pH of the solution was adjusted to 10 using HCl. The solution had a dark orange color and was boiled for 2 min until it turned colorless, then cooled to room temperature. The process of adjusting the pH, boiling, and cooling was repeated two more times. The VO_4 concentration was determined spectroscopically at 265 nm using its molar extinction coefficient of 2,925 M^{-1} cm^{-1}. The solution was stored frozen at −80 °C until usage.

Data Collection and Diffraction Anisotropy Ccorrection. X-ray diffraction data were collected at the Advanced Photon Source (APS-23ID) at 100 K. Diffraction images were processed and scaled with HKL2000 (HKL Research, Inc.) (37). The diffraction data were highly anisotropic, diffracting to 2.2–2.4 Å in the best two directions, and 2.3–3.2 Å in the third direction (Table S2). The scaled data was imported into a diffraction anisotropy server that employs an ellipsoidal truncation and scaling procedure at the high-resolution boundary after elimination of weak or missing reflections (19). The pruned data was then used for structural determination.

Structure Determination. The structures of MBP-MalFGK$_2$ were solved by molecular replacement by PHASER (38) (CCP4 suite) using separate domains of the previously solved MBP-MalFGK$_2$(E159Q) structure as search models. The model was improved by manual building in Coot (39) and initially refined with CNS (40). Further refinement was performed in REFMAC5 (41) with TLS parameters generated by the TLSMD server (42). TLS tensors were analyzed and anisotropic B factors were derived with TLSANL (43).

Figure Preparation. All figures were prepared with the program PyMOL (www.pymol.org).

ACKNOWLEDGMENTS. We thank the staff at the Advanced Photon Source beamline 23-ID for assistance with data collection. This work was supported by National Institutes of Health Grant GM070515 (J.C.) and a postdoctoral fellowship from American Heart Association (M.L.O). J.C is an investigator of the Howard Hughes Medical Institute.

1. Ye J, Osborne AR, Groll M, Rapoport TA (2004) RecA-like motor ATPases—Lessons from structures. *Biochim Biophys Acta* 1659:1–18.
2. Dean M, Rzhetsky A, Allikmets R (2001) The human ATP-binding cassette (ABC) transporter superfamily. *Genome Res* 11:1156–1166.
3. Hollenstein K, Frei DC, Locher KP (2007) Structure of an ABC transporter in complex with its binding protein. *Nature* 446:213–216.
4. Kadaba NS, Kaiser JT, Johnson E, Lee A, Rees DC (2008) The high-affinity *E. coli* methionine ABC transporter: Structure and allosteric regulation. *Science* 321:250–253.
5. Khare D, Oldham ML, Orelle C, Davidson AL, Chen J (2009) Alternating access in maltose transporter mediated by rigid-body rotations. *Mol Cell* 33:528–536.
6. Pinkett HW, Lee AT, Lum P, Locher KP, Rees DC (2007) An inward-facing conformation of a putative metal-chelate-type ABC transporter. *Science* 315:373–377.
7. Ward A, Reyes CL, Yu J, Roth CB, Chang G (2007) Flexibility in the ABC transporter MsbA: Alternating access with a twist. *Proc Natl Acad Sci USA* 104:19005–19010.
8. Aller SG, et al. (2009) Structure of P-glycoprotein reveals a molecular basis for poly-specific drug binding. *Science* 323:1718–1722.
9. Dawson RJ, Locher KP (2006) Structure of a bacterial multidrug ABC transporter. *Nature* 443:180–185.
10. Oldham ML, Khare D, Quiocho FA, Davidson AL, Chen J (2007) Crystal structure of a catalytic intermediate of the maltose transporter. *Nature* 450:515–521.
11. Geourjon C, et al. (2001) A common mechanism for ATP hydrolysis in ABC transporter and helicase superfamilies. *Trends Biochem Sci* 26:539–544.
12. Moody JE, Millen L, Binns D, Hunt JF, Thomas PJ (2002) Cooperative, ATP-dependent association of the nucleotide binding cassettes during the catalytic cycle of ATP-binding cassette transporters. *J Biol Chem* 277:21111–21114.
13. Zaitseva J, Jenewein S, Jumpertz T, Holland IB, Schmitt L (2005) H662 is the linchpin of ATP hydrolysis in the nucleotide-binding domain of the ABC transporter HlyB. *EMBO J* 24:1901–1910.
14. Smith PC, et al. (2002) ATP binding to the motor domain from an ABC transporter drives formation of a nucleotide sandwich dimer. *Mol Cell* 10:139–149.
15. Procko E, Ferrin-O'Connell I, Ng SL, Gaudet R (2006) Distinct structural and functional properties of the ATPase sites in an asymmetric ABC transporter. *Mol Cell* 24:51–62.
16. Dawson RJ, Locher KP (2007) Structure of the multidrug ABC transporter Sav1866 from *Staphylococcus aureus* in complex with AMP-PNP. *FEBS Lett* 581:935–938.
17. Davidson AL, Nikaido H (1991) Purification and characterization of the membrane-associated components of the maltose transport system from *Escherichia coli*. *J Biol Chem* 266:8946–8951.
18. Shimizu T, Johnson KA (1983) Presteady state kinetic analysis of vanadate-induced inhibition of the dynein ATPase. *J Biol Chem* 258:13833–13840.
19. Strong M, et al. (2006) Toward the structural genomics of complexes: Crystal structure of a PE/PPE protein complex from *Mycobacterium tuberculosis*. *Proc Natl Acad Sci USA* 103:8060–8065.
20. Chabre M (1990) Aluminofluoride and beryllofluoride complexes: A new phosphate analogs in enzymology. *Trends Biochem Sci* 15:6–10.
21. Davies DR, Hol WG (2004) The power of vanadate in crystallographic investigations of phosphoryl transfer enzymes. *FEBS Lett* 577:315–321.
22. Sondek J, Lambright DG, Noel JP, Hamm HE, Sigler PB (1994) GTPase mechanism of Gproteins from the 17-Å crystal structure of transducin alpha-GDP-AIF-4. *Nature* 372:276–279.
23. Coleman DE, et al. (1994) Structures of active conformations of Gi alpha 1 and the mechanism of GTP hydrolysis. *Science* 265:1405–1412.
24. Kagawa R, Montgomery MG, Braig K, Leslie AG, Walker JE (2004) The structure of bovine F1-ATPase inhibited by ADP and beryllium fluoride. *EMBO J* 23:2734–2744.
25. Braig K, Menz RI, Montgomery MG, Leslie AG, Walker JE (2000) Structure of bovine mitochondrial F(1)-ATPase inhibited by $Mg^{(2+)}$ ADP and aluminium fluoride. *Structure* 8:567–573.
26. Chen C, et al. (2006) Mitochondrial ATP synthase. Crystal structure of the catalytic F1 unit in a vanadate-induced transition-like state and implications for mechanism. *J Biol Chem* 281:13777–13783.
27. Menz RI, Walker JE, Leslie AG (2001) Structure of bovine mitochondrial F(1)-ATPase with nucleotide bound to all three catalytic sites: Implications for the mechanism of rotary catalysis. *Cell* 106:331–341.
28. Urbatsch IL, et al. (2000) Mutational analysis of conserved carboxylate residues in the nucleotide binding sites of P-glycoprotein. *Biochemistry* 39:14138–14149.
29. Orelle C, Dalmas O, Gros P, Di Pietro A, Jault JM (2003) The conserved glutamate residue adjacent to the Walker-B motif is the catalytic base for ATP hydrolysis in the ATP-binding cassette transporter BmrA. *J Biol Chem* 278:47002–47008.
30. Vergani P, Lockless SW, Nairn AC, Gadsby DC (2005) CFTR channel opening by ATP-driven tight dimerization of its nucleotide-binding domains. *Nature* 433:876–880.
31. Davidson AL, Dassa E, Orelle C, Chen J (2008) Structure, function, and evolution of bacterial ATP-binding cassette systems. *Microbiol Mol Biol Rev* 72:317–364.
32. Urbatsch IL, Sankaran B, Weber J, Senior AE (1995) P-glycoprotein is stably inhibited by vanadate-induced trapping of nucleotide at a single catalytic site. *J Biol Chem* 270:19383–19390.
33. Chen J, Sharma S, Quiocho FA, Davidson AL (2001) Trapping the transition state of an ATP-binding cassette transporter: Evidence for a concerted mechanism of maltose transport. *Proc Natl Acad Sci USA* 98:1525–1530.
34. Orelle C, Ayvaz T, Everly RM, Klug CS, Davidson AL (2008) Both maltose-binding protein and ATP are required for nucleotide-binding domain closure in the intact maltose ABC transporter. *Proc Natl Acad Sci USA* 105:12837–12842.
35. Oldham ML, Chen J (2011) Crystal structure of the maltose transporter in a pretranslocation intermediate state. *Science* 332:1202–1205.
36. Austermuhle MI, Hall JA, Klug CS, Davidson AL (2004) Maltose-binding protein is open in the catalytic transition state for ATP hydrolysis during maltose transport. *J Biol Chem* 279:28243–28250.
37. Otwinowski Z, Minor W (1997) Processing of X-ray diffraction data collected in oscillation mode. *Methods Enzymol* 276:307–326.
38. McCoy AJ, et al. (2007) Phaser crystallographic software. *J Appl Crystallogr* 40:658–674.
39. Emsley P, Cowtan K (2004) Coot: Model-building tools for molecular graphics. *Acta Crystallogr D Biol Crystallogr* 60:2126–2132.
40. Brunger AT (2007) Version 1.2 of the Crystallography and NMR system. *Nat Protoc* 2:2728–2733.
41. Murshudov GN, Vagin AA, Dodson EJ (1997) Refinement of macromolecular structures by the maximum-likelihood method. *Acta Crystallogr D Biol Crystallogr* 53:240–255.
42. Painter J, Merritt EA (2006) TLSMD web server for the generation of multi-group TLS models. *J Appl Crystallogr* 39:109–111.
43. Howlin B, Butler SA, Moss DS, Harris GW, Driessen HPC (1993) TLSANL—TLS parameter-analysis program for segmented anisotropic refinement of macromolecular structures. *J Appl Crystallogr* 26:622–624.